Hindawi
Mathematical Problems in Engineering
Volume 2022, Article ID 3488597, 12 pages
https://doi.org/10.1155/2022/3488597

Research Article

Nonlinear Analysis of the Car-Following Model considering Delay under the V2X Environment

Zhipeng Xu

School of Sciences, Nantong University, Nantong, China

Correspondence should be addressed to Zhipeng Xu; xuzhp@ntu.edu.cn

Received 21 July 2022; Revised 14 November 2022; Accepted 18 November 2022; Published 2 December 2022

Academic Editor: Hongtai Yang

This paper proposes a model that analyzes the delay effect in V2X communication. V2X technology in the intelligent transportation system can realize the exchange of information between vehicles, people, and the environment. Still, more V2X links occupy many channel resources, and the occupation of channel resources leads to longer communication delays. Therefore, based on the optimal velocity of the car-following model, we model the channel delay in the V2X environment. The stability analysis results show that delay increases lead to system instability and traffic congestion. However, if more links are established, that is, the number of vehicles in the vehicle group ahead increases, traffic jams are less likely to occur. The numerical simulation results show that the longer the delay, the more serious the traffic congestion. In addition, we find an apparent phase transition region in the numerical simulation results, which is consistent with the theoretical analysis results. Therefore, in the intelligent transportation system, the delay caused by the complex electromagnetic environment is a factor that cannot be ignored, and thus the allocation of spectrum resources needs to be reasonably arranged. Otherwise, the V2X technology leads to traffic congestion.

1. Introduction

With the development of communication technology, more research combining communication networks and traffic flow has been conducted in recent years. The intelligent transportation system technology represented by V2X is the best option to alleviate the increasing traffic congestion and accidents. In particular, the low-latency characteristics of advanced communication technologies in the technical part of V2X [1]—for example, 5G technology—provide the connection between each vehicle. Additionally, V2X technology can provide the link between environments, such as traffic signal lights, real-time traffic information, and other factors. Therefore, combined with autonomous driving technology, V2X can effectively improve the efficiency of road traffic.

Many scholars [2–8] have investigated various factors and behaviors in intelligent transportation systems, such as delayed feedback [9], two-lane information interaction [10], and other behaviors [11–15]. For example, Ge et al. [11] analyzed the influence of the rear-view mirror effect on driving behavior. The result shows that the cooperative driving behavior of drivers observing vehicles following their vehicle could improve traffic flow stability. Kuang et al. [13] proposed the model considering the influence of the local density in the front view. Analytical and simulation results show that the driving strategy considering multiple vehicles ahead could significantly reduce traffic congestion on the road. In addition, Zhu and Zhang [14] found that referring to the average speed of the vehicle group ahead also had a positive effect on the traffic system. Then, Kuang et al. [15] extended the conclusion by combining the average density and speed. Ngoduy [16] and Luo et al. [17] investigated the effect of the mixed flow with the impact of the penetration of connected and automated vehicles (CAVs) on the traffic flow stability. Jia et al. [18] developed the model for a heterogeneous platoon considering the communication between manual manipulation vehicles and autonomous vehicles. Also, theoretical and numerical analysis showed that the multiclass microscopic model [18] for heterogeneous platoon is linearly stable. Kesting and Treiber [19] analyzed three characteristic time impacts that may affect traffic flow

stability at the micro-level: reaction time, update time, and adaptation time. The reaction time and the update time would affect the traffic system via "short-wavelength mechanisms" as well as transient responses. In contrast, the velocity adaptation time introduces instabilities via collective "long-wavelength mechanisms" like a steady-state response. Yao et al. [20] found that delay time significantly impacts intelligent vehicles because vehicles in a platoon run with such a small gap that even a tiny delay can induce platoon instability. Additionally, Han et al. [21] conducted corresponding research from macro and micro-perspectives. Hence, theoretical analysis has shown that introducing additional information for the vehicle group ahead can significantly improve traffic flow stability.

Many theoretical studies have shown that V2X technology can improve the traffic efficiency of the transportation system, but note that more V2X links may have adverse effects. In particular, many V2X links occupy many electromagnetic spectrum resources, while cell networks have used many frequency bands. Limited wireless channel capacity and resource conflicts also introduce many unpredictable delays into V2X communication. Therefore, in the V2X network, the delay time is a factor that cannot be ignored. Hence, we conduct corresponding research on the impact of delay on traffic flow stability in V2X technology.

2. Model

Bando et al. [22] proposed an ordinary differential equation to study traffic congestion behavior based on the assumption that the driver makes a corresponding speed decision based on the distance from the vehicle ahead. In other words, under the maximum speed limit, the driver accelerates when the distance from the car ahead is enough; otherwise, they decrease the speed conversely. The behavior of the car following can be written as

$$\frac{\mathrm{d}v_n(t)}{\mathrm{d}t} = a\left[V\left(\Delta x_n(t)\right) - v_n(t)\right], \tag{1}$$

where $\Delta x_n(t)$ represents the distance at time t between the n th vehicle and the $(n-1)$th vehicle and v_n represents the nth car's speed correspondingly. a means the sensitivity, reflecting the driver's reaction time. The expected speed $V(\Delta x_n(t))$ related to the gap between two cars can be written as

$$V\left(\Delta x_n(t)\right) = \frac{v_{\max}}{2}\left[\tan h\left(\Delta x_n(t) - h_c\right) + \tan h\left(h_c\right)\right], \tag{2}$$

where h_c and $v_{\max}$ correspond to the maximum safe distance and speed. The velocity $V(\Delta x_n(t))$ rises with the increase of space $\Delta x_n(t)$ and approaches the limited speed $v_{\max}$, also called the optimal velocity.

The optimal velocity car-following model can reflect the nonlinear behavior in the traffic flow system and describe the evolution of traffic congestion. Therefore, based on the optimal velocity model, many scholars have proposed that the model reflects the driving behavior in the intelligent transportation system. Kuang et al. [13] proposed a car-following model considering the density of the vehicle group ahead to discuss the influence of the average density on the system, and the model can be written as

$$\frac{\mathrm{d}v_n(t)}{\mathrm{d}t} = a\left[V\left(\Delta x_n(t), \overline{\Delta x_n(t)}\right) - v_n(t)\right] + \lambda \Delta v_n(t). \tag{3}$$

Compared with the original Bando's model (equation (2)), the average distance of the vehicle ahead $\overline{\Delta x_n(t)}$ is introduced here as

$$\overline{\Delta x_n(t)} = \frac{1}{m}\sum_{l=1}^{m} \Delta x_{n+l}(t). \tag{4}$$

Correspondingly, the optimal velocity can be written as

$$V\left(\Delta x_n(t), \overline{\Delta x_n(t)}\right) = V\left((1-p)\Delta x_n(t) + p\overline{\Delta x_n(t)}\right), \tag{5}$$

where m represents the number of vehicles in the vehicle group ahead and the coefficient p represents the intensity factor of the average distance of the vehicle group ahead. Generally, the coefficient p should not be too large; otherwise, the vehicle collides with the vehicle ahead. Kuang et al. [13] took $p \in [0, 0.3]$ since the influence of current vehicle's headway is more important than the average headway of preceding vehicles group. λ is the responding factor of the velocity difference to avoid unrealistically high acceleration [23].

In the network of vehicles, the allocation of communication channel resources leads to delay, so we extend the model of Kuang by introducing the delay time and propose the following model:

$$\frac{\mathrm{d}v_n(t)}{\mathrm{d}t} = a\left[V\left(\Delta x_n(t), \overline{\Delta x_n(t-\tau)}\right) - v_n(t)\right] + \lambda \Delta v_n(t). \tag{6}$$

The definition of variables is consistent with Kuang et al.'s [13] model (see equation (3)), and the time delay term (τ) is introduced into the average distance between the preceding vehicle groups, reflecting the acquisition and processing delay of the preceding vehicle group. In addition, the ahead vehicle's information is almost instantaneous, so we can ignore the delay. The gap and optimal velocity functions are

$$\overline{\Delta x_n(t-\tau)} = \frac{1}{m}\sum_{l=1}^{m} \Delta x_{n+l}(t-\tau), \tag{7}$$

where $\Delta_{n+k}(t-\tau) = x_{n+k+1}(t-\tau) - x_{n+k}(t-\tau)$. Here, $\overline{\Delta x_n(t-\tau)}$ represents the average distance between preceding vehicles $n+1, n+2, \ldots, n+m$ at time $t-\tau$. Next, the optimal velocity $V(\Delta x_n(t), \overline{\Delta x_n(t-\tau)})$ as well as expected velocity can be obtained as

$$V\left(\Delta x_n(t), \overline{\Delta x_n(t-\tau)}\right) = \frac{v_{\max}}{2}\left(\tan h\left((1-p)\Delta x_n(t) + p\overline{\Delta x_n(t-\tau)} - h_c\right) + \tan h\left(h_c\right)\right). \tag{8}$$

Also, h_c and $v_{\max}$ represent the maximum safe distance and speed. Similarly, we also take $p \in [0, 0.3]$ to ensure that the expected velocity considers the average density of the preceding vehicle group and ignores the essential vehicle ahead distance.

3. Linear Stability Analysis

To discuss the system's stability, that is, the critical condition when uniform flow turns into congestion, we introduce a perturbation into the system to analyze its system robustness. For a system with N vehicles and a road of length L, there must be a stationary solution (the uniform flow) to the equation. Under this condition, all of the vehicles move with the same space $b\,(b = L/N)$ and velocity $V\,(b, b)$. Hence, each vehicle's position $x_n^0(t)$ for steady-state solution at time t can be expressed in the following form:

$$x_n^0(t) = bn + V(b,b)t. \tag{9}$$

If we add a perturbation, $y_n(t)$, that is, $x_n(t) = x_n^0(t) + y_n(t)$, and substitute it into equation (6), then we can obtain

$$\frac{\mathrm{d}^2 y_n}{\mathrm{d}t^2} = a\left[\left((1-p)\Delta y_n(t) + \frac{p}{m}\sum_{l=1}^{m}\Delta y_{n+l}(t-\tau)\right)V'(b) - \frac{\mathrm{d}y_n(t)}{\mathrm{d}t}\right] + \lambda\frac{\mathrm{d}(\Delta y_n(t))}{\mathrm{d}t}. \tag{10}$$

Here, the definitions of $V'(b)$ and $\Delta y_n(t)$ can be written as $V'(b) = [\mathrm{d}V(\Delta x_n)/\mathrm{d}\Delta x_n]|_{\Delta x_n = b}$ and $\Delta y_n(t) = y_{n+1}(t) - y_n(t)$.

Next, let $y_n = \exp(ikn + zt)$; that is, express the perturbation in the form of dispersion and substitute this equation into formula (10). Then, we can get

$$z^2 - z\left[\lambda\left(\mathrm{e}^{ik} - 1\right) - a\right] - a\left[(1-p)\left(\mathrm{e}^{ik} - 1\right)V'(b) + \frac{p}{m}\left(\mathrm{e}^{ik(m+1)-z\tau} - \mathrm{e}^{ik-z\tau}\right)V'(b)\right] = 0. \tag{11}$$

The parameter z can be expanded as

$$z = ikz_1 + (ik)z_2 + \cdots. \tag{12}$$

By substituting z into equation (11), we can obtain first and second-order expansions of ik as follows:

$$z_1 = V'(b)$$
$$z_2 = \frac{1}{2}\left(1 + p\left(1 + m - 2z_1\tau\right)\right)V'(b) + \frac{1}{a}\left(z_1\lambda - z_1^2\right). \tag{13}$$

According to the analysis of stability theory, when $z_2 < 0$, the disturbance decays exponentially and tends to be stable. Corresponding to the traffic flow, the speed fluctuation of individual vehicles does not cause traffic congestion. Conversely, when $z_2 > 0$, the velocity fluctuations of cars can easily cause congestion in the entire system. Therefore, letting $z_2 = 0$, we can get the critical condition of system stability, that is, the neutral stability condition:

$$a = \frac{2\left[V'(b) - \lambda\right]}{1 + p + mp - 2p\tau V'(b)}. \tag{14}$$

To keep the system stable, the sensitivity coefficient needs to satisfy the following condition:

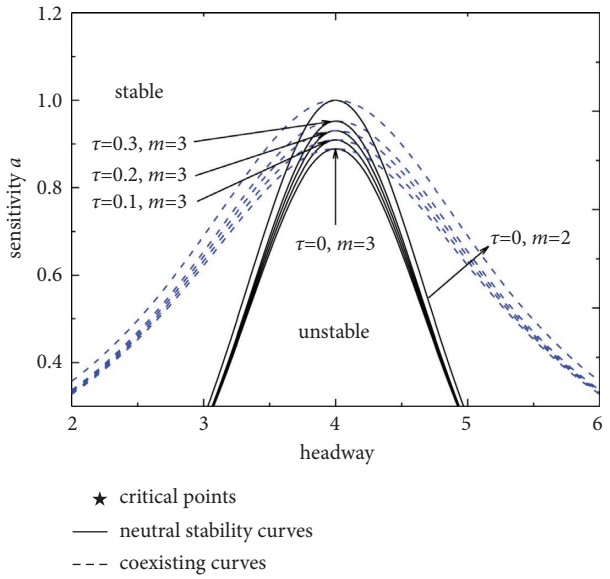

Figure 1: The phase space of headway density.

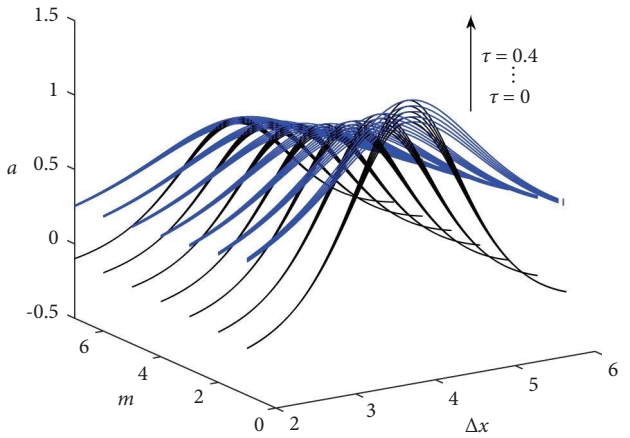

Figure 2: The phase space of headway density with different m and τ values.

$$a > \frac{2\left[V'(b) - \lambda\right]}{1 + p + mp - 2p\tau V'(b)}. \tag{15}$$

When $\tau = 0$, the stability results are consistent with Kuang et al.'s [13] results; also, in the condition of $p = 0$, $\tau = 0$, this model reduces into Jiang et al.'s [23] full-velocity difference model.

Figure 1 shows the parameter space phase diagram of vehicle distance (Δx) and the sensitivity coefficient a, where $\tau = 0.3$, $p = 0.3$, and $\lambda = 0.1$. The region in the figure can be divided into three areas: the stable area, the metastable area, and the unstable area. The system has strong robustness when the parameter space $(\Delta x, a)$ is located in the stable region. At higher sensitivities or lower vehicle densities, random disturbances between individual vehicle speeds and

vehicle spacing eventually dissipate, and the traffic flow can remain stable. Compared with Kuang's results, we can find that the introduction of delay (τ) increases the area of the unstable region, which is consistent with the fact that delay leads to system instability. Importantly, in V2X systems, especially when the electromagnetic environment becomes more complex, the delay is a nonnegligible factor. In Ge et al.'s [24] results, the number of vehicles in the current vehicle group $m = 3$ is the optimal state for cooperative driving, so we only analyze it with $m = 3$ in Figure 1.

Figure 2 shows the stability curves under different m values, and we notice that as the number of vehicles in the vehicle group ahead (m) increases, the instability area shrinks. This result shows that the stability of the traffic flow system can be promoted if more vehicles ahead are considered. However, under the same m, as the delay time (τ) increases, the unstable region also increases, but the gap becomes smaller as m increases. The analysis also reminds us that when τ increases in the intelligent transportation system, we can introduce more reference vehicle information in exchange for improving system stability.

4. Nonlinear Analysis

The theoretical analysis in most literature shows that the propagation process of density waves represents the traffic congestion behavior so that these equations can be expanded into the corresponding Burgers, KdV, TDGL, and mKdV equations under specific conditions [25–31]. Here, we only discuss the case of the mKdV equation. We rewrite equation (6) in the form of $\mathrm{d}^2x_{n+1}(t)/\mathrm{d}t^2 - \mathrm{d}^2x_n(t)/\mathrm{d}t^2$ to get the following equation:

$$\frac{\mathrm{d}^2\Delta x_n(t)}{\mathrm{d}t^2} = a\left[V\left((1-p)\Delta x_{n+1}(t) + \frac{p}{m}\sum_{l=1}^{m}\Delta x_{n+l+1}(t-\tau)\right) - V\left((1-p)\Delta x_n(t) + \frac{p}{m}\sum_{l=1}^{m}\Delta x_{n+l}(t-\tau)\right) - \frac{\mathrm{d}\Delta x_n(t)}{\mathrm{d}t}\right] + \lambda\left(\frac{\mathrm{d}\Delta x_{n+1}(t)}{\mathrm{d}t} - \frac{\mathrm{d}\Delta x_n(t)}{\mathrm{d}t}\right). \tag{16}$$

Then, we introduce the slow variables X and T as

$$X = \varepsilon(j + bt), T = \varepsilon^3 t, 0 < \varepsilon \le 1. \tag{17}$$

Among them, b is the parameter related to the critical point. Next, we introduce the function $R(X,T)$ and redefine the vehicle distance $\Delta x_n(t)$ as follows:

$$\Delta x_n(t) = h_c + \varepsilon R(X,T). \tag{18}$$

Substituting equations (17) and (18) into equation (16) and then performing the reductive perturbation method [11, 13, 15, 24, 25], we get

$$\frac{\mathrm{d}\Delta x_n(t)}{\mathrm{d}t} = b\varepsilon^2\partial_X R + \varepsilon^4\partial_T R, \tag{19}$$

$$\frac{\mathrm{d}^2\Delta x_n(t)}{\mathrm{d}t^2} = b^2\varepsilon^3\partial_X^2 R + 2b\varepsilon^5\partial_X\partial_T R, \tag{20}$$

$$\frac{\mathrm{d}\Delta x_{n+1}(t)}{\mathrm{d}t} = b\varepsilon^2\partial_X R + b\varepsilon^3\partial_X^2 R + \varepsilon^4\left(\frac{1}{2}b\partial_X^3 R + \partial_T R\right) + \varepsilon^5\left(\frac{1}{6}b\partial_X^4 R + \partial_X\partial_T R\right), \tag{21}$$

$$\Delta x_n(t-\tau) = h_c + \varepsilon R - b\varepsilon^2\tau\partial_X R + \frac{1}{2}b^2\varepsilon^3\tau^2\partial_X^2 R + \varepsilon^4\left(-\tau\partial_T R - \frac{1}{6}b^3\tau^3\partial_X^3 R\right) + \varepsilon^5\left(b\tau^2\partial_X\partial_T R + \frac{1}{24}b^4\tau^4\partial_X^4 R\right), \tag{22}$$

$$\begin{aligned}\frac{1}{m}\sum_{l=1}^{m}\Delta x_{n+l}(t-\tau) = h_c + \varepsilon R + \frac{\varepsilon^2}{m}\left(-bm\tau + \sum_{l=1}^{m} l\right)\partial_X R \\ + \frac{\varepsilon^3}{2m}\left(bm\tau(b\tau - 1 - m) + \sum_{l=1}^{m} l^2\right)\partial_X^2 R \\ + \frac{\varepsilon^4}{6m}\Big(-\frac{1}{2}bm\tau\Big(2b^2\tau^2 - 3b(m+1)\tau + 2m^2 + 3m + 1\Big) \\ + \sum_{l=1}^{m} l^3\Big)\partial_X^3 R - \varepsilon^4\tau\partial_T R - \varepsilon^5\Big(\frac{1}{2}\tau(-2b\tau + m + 1)\Big)\partial_X\partial_T R \\ + \frac{\varepsilon^5}{24m}\Big(-bm\tau(-b\tau + m + 1)\Big(-bm\tau + b\tau(b\tau - 1) + m^2 + m\Big) \\ + \sum_{l=1}^{m} l^4\Big)\partial_X^4 R,\end{aligned} \tag{23}$$

$$\begin{aligned}&\frac{1}{m}\sum_{l=1}^{m}\Delta x_{n+l+1}(t-\tau) \\ &= h_c + \varepsilon R + \frac{\varepsilon^2}{m}\left(-bm\tau + \sum_{l=1}^{m}(l+1)\right)\partial_X R \\ &+ \frac{\varepsilon^3}{2m}\left(bm\tau(b\tau - 3 - m) + \sum_{l=1}^{m}(l+1)^2\right)\partial_X^2 R \\ &+ \frac{\varepsilon^4}{6m}\Big(-\frac{1}{2}bm\tau\Big(m(9 - 3b\tau) + b\tau(2b\tau - 9) + 2m^2 + 13\Big) \\ &+ \sum_{l=1}^{m}(l+1)^3\Big)\partial_X^3 R - \varepsilon^4\tau\partial_T R \\ &- \varepsilon^5\Big(\frac{1}{2}\tau(-2b\tau + m + 3)\Big)\partial_X\partial_T R \\ &+ \frac{\varepsilon^5}{24m}\Big(-bm\tau(-b\tau + m + 3)\Big(m(3 - b\tau) + b\tau(b\tau - 3) + m^2 + 4\Big) \\ &+ \sum_{l=1}^{m}(l+1)^4\Big)\partial_X^4 R,\end{aligned} \tag{24}$$

$$\begin{aligned}&V\left((1-p)\Delta x_n(t) + \frac{p}{m}\sum_{l=1}^{m}\Delta x_{n+l}(t-\tau)\right) \\ &= V(h_c) + \left((1-p)\Delta x_n(t) + \frac{p}{m}\sum_{l=1}^{m}\Delta x_{n+l}(t-\tau) - h_c\right)V' \\ &+ \frac{1}{6}\left((1-p)\Delta x_n(t) + \frac{p}{m}\sum_{l=1}^{m}\Delta x_{n+l}(t-\tau) - h_c\right)^3 V''',\end{aligned} \tag{25}$$

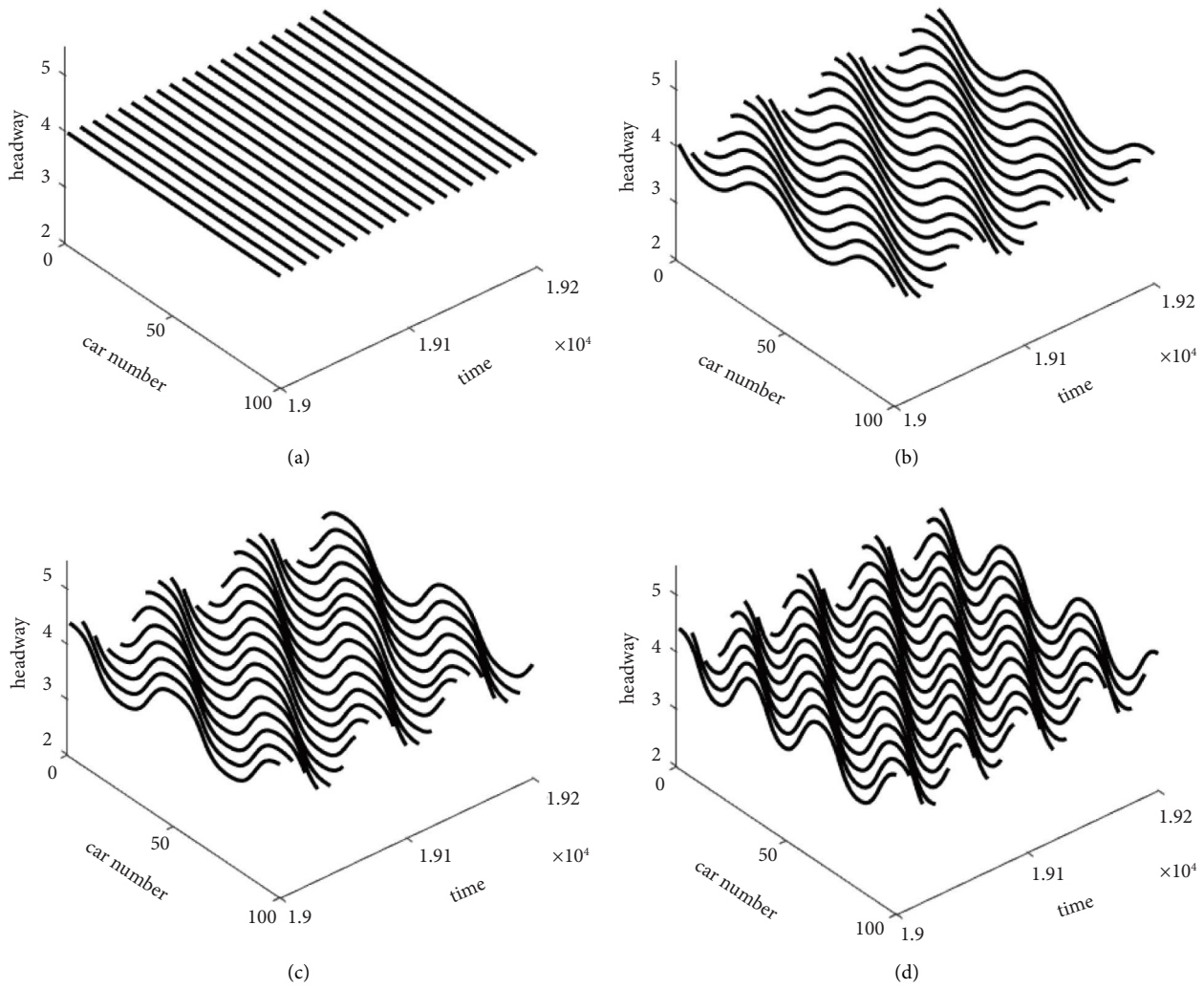

Figure 3: Space-time evolution of the headway for different values of α when $F(\Delta x) = -2(\Delta x - 1)$. (a)$\tau = 0$. (b)$\tau = 0.1$. (c)$\tau = 0.2$. (d)$\tau = 0.3$.

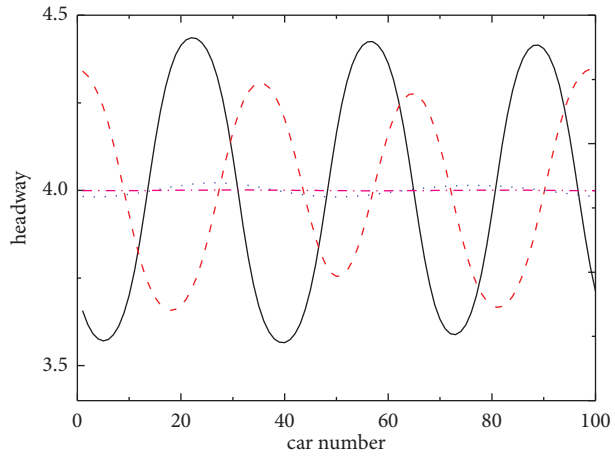

Figure 4: The distribution of density waves when $t = 19200$.

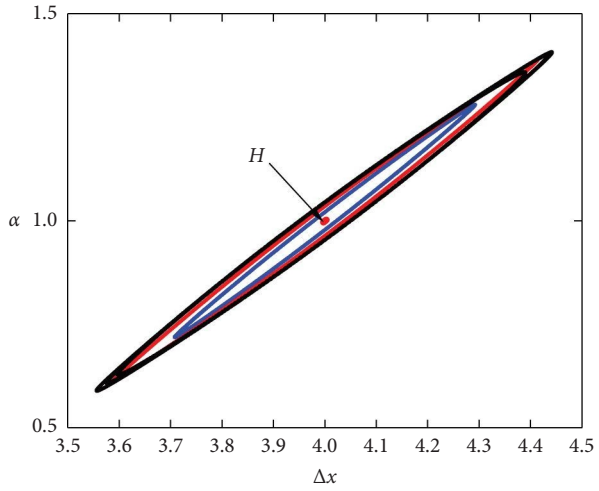

Figure 5: The hysteresis loop in phase space $(\Delta x, v)$ for $\tau = 0, 0.1, 0.2, 0.3$.

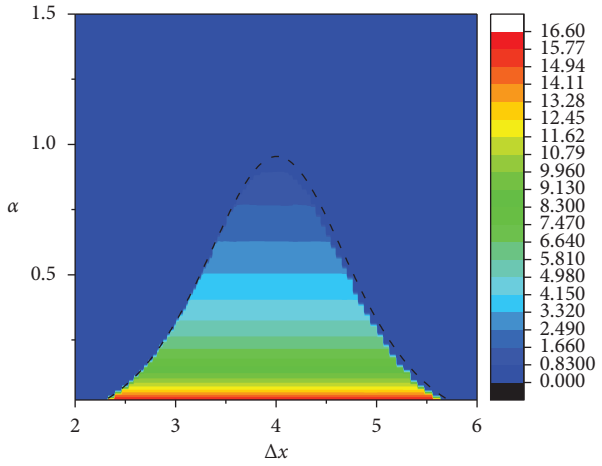

Figure 6: Heatmap of $|\max(\Delta x_n) - \min(\Delta x_n)|$ for $t = 20000$ in the phase space of $(\Delta x, \alpha)$.

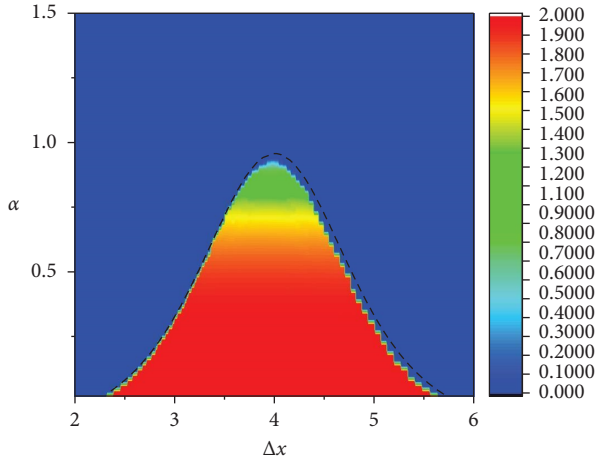

Figure 7: Heatmap of $|\max(\Delta v_n) - \min(\Delta v_n)|$ for $t = 20000$ in the phase space of $(\Delta x, \alpha)$.

$$V\left((1-p)\Delta x_{n+1}(t)+\frac{p}{m}\sum_{l=1}^{m}\Delta x_{n+l+1}(t-\tau)\right)$$
$$=V(h_c)+\left((1-p)\Delta x_{n+1}+\frac{p}{m}\sum_{l=1}^{m}\Delta x_{n+l+1}(t-\tau)-h_c\right)V' \tag{26}$$
$$+\frac{1}{6}\left((1-p)\Delta x_{n+1}+\frac{p}{m}\sum_{l=1}^{m}\Delta x_{n+l+1}(t-\tau)-h_c\right)^3 V'''.$$

Here, the definition of V' and V''' can be written as

$$V'=V'(h_c)=\left[\frac{\mathrm{d}V\left((1-p)\Delta x_n+p\overline{\Delta x_n}\right)}{\mathrm{d}\Delta x_n}\right]\Big|_{\Delta x_n=h_c,\overline{\Delta x_n}=h_c},$$
$$V'''=V'''(h_c)=\left[\frac{\mathrm{d}^3V\left((1-p)\Delta x_n+p\overline{\Delta x_n}\right)}{\mathrm{d}^3\Delta x_n}\right]\Big|_{\Delta x_n=h_c,\overline{\Delta x_n}=h_c}. \tag{27}$$

Next, we substitute equations (20)–(27) into equation (16) and get

$$\varepsilon^2(b-V')\partial_X R+\varepsilon^3\left[\frac{b(b-\lambda)}{a}-\frac{(mp+p+1-2bp\tau)V'}{2}\right]\partial_X^2 R$$
$$+\varepsilon^4\left\{\partial_T R-\left[\frac{\left(m^2p+3mp+2p-3bpm(2+m)\tau+1\right)V'}{6}+\frac{b\lambda}{2a}\right]\partial_X^3 R-\frac{V'''}{6}\partial_X R^3\right\}$$
$$+\varepsilon^5\left\{\left(\frac{2b-\lambda}{a}+2p\tau V'\right)\partial_X\partial_T R-\frac{(mp+p+1)V'''}{12}\partial_X^2 R^3\right. \tag{28}$$
$$+\frac{1}{24a}\left(-4b\lambda-a\left(1+p\left(m^2(4-4b\tau)+6m(b\tau-1)^2+m^3+3\right.\right.\right.$$
$$\left.\left.\left.-4b\tau(b\tau(b\tau-3)+3)\right)\right)\partial_X^4 R\right\}=0.$$

Let $a_c=a(1+\varepsilon^2)$ and $b=V'$; then, the terms in equation (28) of ε^2 and ε^3 can be eliminated, and we finally get the equation for the fourth-order and fifth-order terms of ε as

$$\varepsilon^4\left(\partial_T R-g_1\partial_X^3 R+g_2\partial_X R^3\right)+\varepsilon^5\left(g_3\partial_X^2 R+g_4\partial_X^4 R+g_5\partial_X^2 R^3\right)=0. \tag{29}$$

Here, each coefficient can be written as

$$
\begin{aligned}
g_1 &= \left(\frac{1}{6} + \frac{p(1+m)(2+m)}{6} + \frac{\lambda}{2a_c} + \frac{p\tau V'(\tau V' - 2 - m)}{2}\right)V', \\
g_2 &= -\frac{1}{6}V''', \\
g_3 &= \frac{1 + p + mp - 2p\tau V'}{2}V', \\
g_4 &= -\frac{1}{6a^2}\left((\lambda - (ap\tau + 2)V')\left(3ap\tau V'(\tau V' - m - 2) + a(m+1)(m+2)p + a + 3\lambda\right)\right) \\
&\quad -\frac{1}{24a}\left(a + 4\lambda + ap\left((m+1)(m(m+3)+3) + 2\tau V'(-2m(m+3) - 6\right.\right. \\
&\quad \left.\left. + \tau V'(-2\tau V' + 3m + 6)\right)\right), \\
g_5 &= -\frac{a_c(p + mp + 1) - 4(1 + ap\tau)V' + 2\lambda}{12a_c}V'''.
\end{aligned}
\tag{30}
$$

To obtain the standard mKdV equation, including the high-order ε, we can introduce the transformation as follows:

$$
T = \frac{T'}{g_1}, R(X,T) = \sqrt{\frac{g_1}{g_2}}R'(X,T'). \tag{31}
$$

The obtained mKdV equation including $O(\varepsilon)$ can be written as

$$
\partial_{T'}R' - \partial_X^3 R' + \partial_X R'^3 + \varepsilon M[R'] = 0. \tag{32}
$$

The term of $M[R']$ is

$$
M[R'] = \frac{1}{g_1}\left[g_3\partial_X^2 R' + g_4\partial_X^4 R' + \frac{g_1 g_5}{g_2}\partial_X^2 R'^3\right]. \tag{33}
$$

If we neglect $O(\varepsilon)$, then we can get the kink-antikink solution of the standard mKdV equation as

$$
R_0'(X,T') = \sqrt{c}\tan h\left[\sqrt{\frac{c}{2}}(X - cT')\right]. \tag{34}
$$

To determine the speed velocity (c) in equation (34), we can introduce the soluble condition as

$$
(R_0', M[R_0']) \equiv \int_{-\infty}^{+\infty} \mathrm{d}X R_0' M[R_0'] = 0. \tag{35}
$$

In equation (35), we have $M[R_0'] = M[R_0]$. By integrating equation (35), we can calculate c for the kink-antikink wave as

$$
c = \frac{5g_2 g_3}{2g_2 g_4 - 3g_1 g_5}. \tag{36}
$$

Finally, we get the solution for the mKdV equation as

$$
R(X,T) = \sqrt{\frac{g_1 c}{g_2}}\tanh\sqrt{\frac{c}{2}}(X - cg_1 T). \tag{37}
$$

By substituting equation (37) into equation (18), we get the kink-antikink solution of the headway as

$$
\Delta x_n = h_c + \sqrt{\frac{g_1 c}{g_2}\left(\frac{a_c}{a} - 1\right)}\tanh\sqrt{\frac{c}{2}\left(\frac{a_c}{a} - 1\right)}\left[n + \left(1 - cg_1\left(\frac{a_c}{a} - 1\right)t\right)\right]. \tag{38}
$$

The amplitude for the kink-antikink wave can be written as

$$
A = \sqrt{\frac{g_1 c}{g_2}\left(\frac{a_c}{a} - 1\right)}. \tag{39}
$$

The coexisting curves can expressed as $\Delta x_n = h_c + A$, as shown in Figures 1 and 2.

5. Numerical Simulation

We simulate the equation to verify the theoretical analysis results. Here, we use periodic boundary conditions, and the initial conditions are as follows:

$$
\begin{aligned}
&\Delta x_n(0) = \Delta x_n(1) = \Delta x_0, \text{for } n \neq 0.5N, 0.5N + 1, \\
&\Delta x_n(0) = \Delta x_n(1) = \Delta x_0 + 0.1, \text{for } n = 0.5N,
\end{aligned}
\tag{40}
$$

$$
\Delta x_n(0) = \Delta x_n(1) = \Delta x_0 - 0.1, \text{for } n = 0.5N + 1, \tag{41}
$$

where Δx_0 represents the vehicle distance of the uniform solution and N is the total number of vehicles. We introduce a small disturbance with the length of 0.1 m, as shown in equation (41). In addition, other parameters of the system are $N = 100, \Delta x_0 = 4.0, p = 0.2, \lambda = 0.2$, and $a = 0.88$.

Figure 3 gives the phase diagram results of the space–time evolution when $19000 < t < 19200$, where Figures 3(a)–3(d) represent $\tau = 0, 0.1, 0.2, 0.3$. When τ is relatively small, the disturbance introduced in equation (6) will disappear. The disturbance is amplified when τ is rather large and the stability condition is not met. Finally, the propagation of the density wave is formed, showing the stop-and-go phenomenon. The phenomenon is well described by expanding the model to a kink-antikink wave solution of the mKdV equation at the critical point. In addition, with the increase of τ, the amplitude of the density wave also increases, which also means that the rise of the delay in the complex environment leads to traffic congestion. However, the accumulation of vehicles caused by traffic congestion further worsens the transmission delay, and the positive feedback deteriorates the traffic congestion. Therefore, the intelligent transportation system needs delay control and a good electromagnetic environment.

Figure 4 shows the distribution of density waves when $t = 19200$. When $\tau = 0.3$, the amplitude becomes more significant in that the distance between vehicles becomes larger. When τ decreases, the amplitude gradually decreases until a steady state of uniform flow is maintained. The steady-state system with low delay time can suppress the disturbance, so the minor communication delay helps improve the traffic efficiency of the intelligent transportation system.

Figure 5 shows the hysteresis loop in phase space $(\Delta x, v)$ at different τ values, where the x-axis represents the distance between vehicles, and the y-axis represents the speed. It can be observed from the phase diagram that after a long-term evolution, the speed and the distance between cars exhibit oscillation, and the amplitude of the oscillation shrinks as τ decreases until $\tau = 0$ converges to the H point. Therefore, the size characteristics of the hysteresis loop are consistent with the theoretical analysis results.

Finally, to determine the accuracy of the stability analysis, we define the difference between the maximum and minimum headways in the system when $t = 20000$ steps, as follows:

$$\delta x = \max\left(\Delta x_n\right) - \min\left(\Delta x_n\right). \tag{42}$$

Similarly, we can define the maximum and minimum speed difference as

$$\delta v = \max\left(v_n\right) - \min\left(v_n\right). \tag{43}$$

We are curious whether the numerical results on the region but not specified points are consistent with the theoretical analysis results. Hence, simulations on the parameter space with $\Delta x \in [2, 6] \times a \in [0.02, 1.5]$ are performed. From the phase diagram of the distance difference between vehicles, shown in Figure 6, it can be found that there is a prominent phase transition area, and the black dotted line corresponds to its neutral stability curve. It can be seen that the results of the numerical simulation throughout the parameter space are consistent with the results of the theoretical analysis. The blue area represents the uniform free flow, while the area below the curve represents the occurrence of traffic congestion. As the sensitivity coefficient decreases, the gap between the maximum and minimum distance between vehicles becomes larger. Also, in Figure 7, we observe the phase transition, but the maximum and minimum speed difference caused by the speed limit is only about 2.

In addition, we observe that the phase diagrams shown in Figures 6 and 7 show symmetry with $\Delta x = 4$ as the symmetry axis. Under the same sensitivity coefficient a, traffic congestion still occurs even if the vehicle density is low. This also shows that there is no absolute relationship between road congestion and the level of vehicle density. Even so, this significantly relates to the driver's reaction speed and driving behavior. In the case of manual driving, it is difficult to improve the sensitivity coefficient (a), while automatic driving can effectively overcome the problems of decreased sensitivity caused by long-term driving and inattention. Therefore, it can be found that autonomous driving in the V2X environment can effectively improve road traffic efficiency and reduce congestion.

6. Conclusions

With the rapid development of artificial intelligence, self-driving vehicles have become a reality. 5G technology has been shown to effectively improve the speed of mobile communication networks and reduce communication delays, laying the foundation for the realization of automotive networks. Therefore, this paper introduces the communication delay based on the average density of the vehicle group ahead in the intelligent transportation system and analyzes the influence of the communication delay on traffic flow composed of intelligent vehicles. The theoretical analysis results show that excessive communication delay causes instability in the traffic system. Even so, if the number of cars in the vehicle group is increased, we can effectively reduce the possibility of traffic jams caused by the communication delay.

Numerical simulation results verify our conclusions; at the same time, we conduct large-scale numerical simulations for the results of stability analysis. The numerical results are consistent with the theoretical analysis results and exhibit an obvious phase transition phenomenon, and the phase diagram shows a high degree of symmetry. This indicates that road congestion is mainly caused by driving behavior and to a lesser degree by too many vehicles. Therefore, fast response and consistent driving behavior in an intelligent transportation system can effectively alleviate traffic congestion.

Autonomous driving is developing rapidly, which inspired us to analyze possible factors in the independent driving system through theoretical analysis and conduct simulation accordingly.

Data Availability

The simulated data used to support the findings of this study are available from the corresponding author upon request.

Conflicts of Interest

The author declares that there are no conflicts of interest regarding the publication of this paper.

Acknowledgments

This study was supported by Nantong Science & Technology Research Plan (no. JC2021133).

References

[1] S. Chen, J. Hu, Y. Shi et al., "Vehicle-to-everything (v2x) services supported by LTE-based systems and 5g," *IEEE Communications Standards Magazine*, vol. 1, no. 2, pp. 70–76, 2017.

[2] D. Thuan Do, M. Sang Van Nguyen, M. Voznak, K. Andres, and J. Neuman de Souza, "Performance analysis of clustering car-following v2x system with wireless power transfer and massive connections," *IEEE Internet of Things Journal*, vol. 1, no. 1, 2021.

[3] G. Peng and Q. Li, "Nonlinear analysis of the individual difference corresponding to honk effect for car-following theory under v2x environment," *International Journal of Modern Physics C*, vol. 31, no. 11, Article ID 2050157, 2020.

[4] J. Han, J. Zhang, X. Wang, Y. Liu, Q. Wang, and F. Zhong, "An extended car-following model considering generalized preceding vehicles in v2x environment," *Future Internet*, vol. 12, no. 12, p. 216, 2020.

[5] Y. Li, W. Chen, P. Srinivas, and Y. Wang, "Platoon control of connected multi-vehicle systems under v2x communications: design and experiments," *IEEE Transactions on Intelligent Transportation Systems*, vol. 21, no. 5, pp. 1891–1902, 2020.

[6] G.-H. Peng, Te-Ti Jia, H. Kuang, H.-Li Tan, and T. Chen, "A novel car-following model by sharing cooperative information transmission delayed effect under v2x environment and its additional energy consumption," *Chinese Physics B*, vol. 31, no. 5, Article ID 058901, 2022.

[7] W. Xu, N. Li, W. Liang, and H. Liu, "Dissipation characteristics of vehicle queue in v2x environment based on improved car-following model," *Mathematical Problems in Engineering*, vol. 2022, pp. 1–17, 2022.

[8] Z. Tong, Y. Li, and G. Peng, "Impact of the self-interruption probability involving the anticipation optimal velocity on traffic stability for car-following theory under v2x environment," *IEEE Access*, vol. 9, pp. 111456–111462, 2021.

[9] Y. Sun, H. Ge, and R. Cheng, "An extended car-following model under v2v communication environment and its delayed-feedback control," *Physica A: Statistical Mechanics and Its Applications*, vol. 508, pp. 349–358, 2018.

[10] H. Ou and T.-Q. Tang, "An extended two-lane car-following model accounting for inter-vehicle communication," *Physica A: Statistical Mechanics and Its Applications*, vol. 495, pp. 260–268, 2018.

[11] H. X. Ge, H. B. Zhu, and S. Q. Dai, "Effect of looking backward on traffic flow in a cooperative driving car following model," *The European Physical Journal B*, vol. 54, no. 4, pp. 503–507, 2006.

[12] J. Zhao and Li Peng, "An extended car-following model with consideration of speed guidance at intersections," *Physica A*, vol. 461, 2016.

[13] H. Kuang, Z.-P. Xu, X.-Li Li, and S.-M. Lo, "An extended car-following model accounting for the average headway effect in intelligent transportation system," *Physica A: Statistical Mechanics and Its Applications*, vol. 471, pp. 778–787, 2017.

[14] W.-X. Zhu and Li.-D. Zhang, "A new car-following model for autonomous vehicles flow with mean expected velocity field," *Physica A: Statistical Mechanics and Its Applications*, vol. 492, pp. 2154–2165, 2018.

[15] H. Kuang, M.-T. Wang, F.-H. Lu, Ke-Zhao Bai, and X.-Li Li, "An extended car-following model considering multi-anticipative average velocity effect under v2v environment," *Physica A: Statistical Mechanics and Its Applications*, vol. 527, Article ID 121268, 2019.

[16] D. Ngoduy, "Analytical studies on the instabilities of heterogeneous intelligent traffic flow," *Communications in Nonlinear Science and Numerical Simulation*, vol. 18, no. 10, pp. 2699–2706, 2013.

[17] R. Luo, Q. Gu, T. Xu, H. Hao, and Z. Yao, "Analysis of linear internal stability for mixed traffic flow of connected and automated vehicles considering multiple influencing factors," *Physica A: Statistical Mechanics and Its Applications*, vol. 597, Article ID 127211, 2022.

[18] D. Jia, D. Ngoduy, and H. L. Vu, "A multiclass microscopic model for heterogeneous platoon with vehicle-to-vehicle communication," *Transportation Business: Transport Dynamics*, vol. 7, no. 1, pp. 311–335, 2018.

[19] A. Kesting and M. Treiber, "How reaction time, update time, and adaptation time influence the stability of traffic flow," *Computer-Aided Civil and Infrastructure Engineering*, vol. 23, no. 2, pp. 125–137, 2008.

[20] Z. Yao, T. Xu, Y. Jiang, and R. Hu, "Linear stability analysis of heterogeneous traffic flow considering degradations of connected automated vehicles and reaction time," *Physica A: Statistical Mechanics and Its Applications*, vol. 561, Article ID 125218, 2021.

[21] J. Han, H. Shi, L. Chen, H. Li, and X. Wang, "The car-following model and its applications in the v2x environment: a historical review," *Future Internet*, vol. 14, no. 1, p. 14, 2021.

[22] M. Bando, K. Hasebe, A. Nakayama, A. Shibata, and Y. Sugiyama, "Dynamical model of traffic congestion and numerical simulation," *Physical Review A*, vol. 51, pp. 1035–1042, 1995.

[23] R. Jiang, Q. Wu, and Z. Zhu, "Full velocity difference model for a car-following theory," *Physical Review A*, vol. 64, no. 1, Article ID 017101, 2001.

[24] H. X. Ge, S. Q. Dai, Y. Xue, and L. Y. Dong, "Stabilization analysis and modified kortewegde vries equation in a cooperative driving system," *Physical Review A*, vol. 71, Article ID 066119, 2005.

[25] H. X. Ge, R. J. Cheng, and S. Q. Dai, "Kdv and kink-antikink solitons in car-following models," *Physica A*, vol. 357, no. 3-4, pp. 466–476, 2005.

[26] F. Liu, R. Cheng, P. Zheng, and H. Ge, "TDGL and mKdV equations for car-following model considering traffic jerk," *Nonlinear Dynamics*, vol. 83, pp. 793–800, 2015.

[27] H.-X. Ge, P.-J. Zheng, S.-M. Lo, and R.-J. Cheng, "TDGL equation in lattice hydrodynamic model considering driver's physical delay," *Nonlinear Dynamics*, vol. 76, no. 1, pp. 441–445, 2013.

[28] F. Lv, H.-B. Zhu, and H.-X. Ge, "TDGL and mKdV equations for car-following model considering driver's anticipation," *Nonlinear Dynamics*, vol. 77, no. 4, pp. 1245–1250, 2014.

[29] H. Ge, Y. Zhang, H. Kuang, and S.-M. Lo, "The tdgl equation for car-following model with consideration of the traffic interruption probability," *International Journal of Modern Physics C*, vol. 23, no. 07, Article ID 1250053, 2012.

[30] T. Nagatani, "Tdgl and mkdv equations for jamming transition in the lattice models of traffic," *Physica A*, vol. 264, pp. 581–592, 1999.

[31] T. Nagatani, "Time-dependent ginzburg-landau equation for the jamming transition in traffic flow," *Physica A*, vol. 258, no. 1-2, pp. 237–242, 1998.